# Structural and Optical Properties of Rare Earth Nano-Crystalline Oxides Embedded in Polymethyl Methacrylate

S. Tabanli[*], G. Bilir[**], M. Erdem[***], G. Eryurek[****]

[*]Department of Physics Engineering, Istanbul Technical University, Istanbul, TURKEY, tabanlisevcan@itu.edu.tr
[**]Department of Physics, Kafkas University, Kars, TURKEY, bilir@bc.edu
[***]Department of Physics, Marmara University, Istanbul, TURKEY, merdem@marmara.edu.tr
[****]Department of Physics Engineering, Istanbul Technical University, Istanbul, TURKEY, gozenl@itu.edu.tr

## ABSTRACT

In this study, various sizes of rare earth oxide nano-crystalline powders ($Nd_2O_3$ and $Er_2O_3$) were doped into polymethyl methacrylate (PMMA) host material which were synthesized using the thermal decomposition method. The structural characterization of the composites were made using X-ray diffraction. The spectroscopic measurements such as absorption and emission spectra were conducted.

PMMA is an amorphous, thermoplastic polymer with an optical transparency region from 300 nm to 2800 nm. Beyond the excellent optical properties, PMMA shows superior resistance to laser, high mechanical strength and ease of synthesis thus, this properties make it suitable for the production of elastic polymer material that emits light.

***Keywords***: PMMA, rare earth oxides, XRD, absorption, emission

## 1 ıNTRODUCTıON

It is known that trivalent rare earth ions (RE) have several unique spectroscopic properties such as relatively good photoluminescence (PL) efficiency, sharp emission and absorption spectrum. Due to the its important features, materials doped with rare-earth ions have been widely used for lighting, displays, optical communications, fluorescent biolabels, solid state lasers [1]. Converting the lanthanide complexes into the processeable systems has been extremelly challenging. However polymer materials provide synthetic and processing options that are not available with other classes of optical materials such as processing flexibility, relatively small amount of wasted materials (environmental friendly), excellent mechanical properties, easily processability, the compatibility with flexible substrates, better control in doping level, and high laser damage thresholds. This motivates the search for polymer based optical systems that would enable easier fabrication at low cost for larger networks of multiple channel systems. RE oxides doped plastic laser host materials are easily drawn into flexible optical fibers for photonic applications such as laser systems, optical communication devices, polymer optical fiber amplifier and integrated polymer waveguide [2, 3].

In this study, we obtained a transparent polymer of PMMA with embedded nano-crystalline $Nd_2O_3$ and $Er_2O_3$ powder. Our aim is to investigate the effect of the rare earth oxide dopant and the heat treatment on the structure and optical properties of the materials to obtain an efficient infrared emission under 808 nm and 980 nm excitation laser for $Nd_2O_3$ and $Er_2O_3$, repectively.

## 2 EXPERıMENTAL

### 2.1 Materials Preparation

**Synthesis of $Nd_2O_3$ and $Er_2O_3$ nanocrystalline oxide:** Nanosized $Nd_2O_3$ and $Er_2O_3$ nanocrystalline powders were prepared by thermal decomposition. Neodymium(III) nitrate hexahydrate $Nd(NO_3)_3.6H_2O$ and alginic acid sodium salt (low viscosity, 250 cps, 2% solution in water) were used for synthesis of $Nd_2O_3$ nanocrystals. Erbium(III) nitrate pentahydrate $ErN_3O_9.5H_2O$ and alginic acid sodium salt (low viscosity, 250 cps, 2% solution in water) were used for synthesis of $Er_2O_3$ nanocrystals. All chemicals used were of analytical grade and were used as received without any further purification and were obtained from Sigma-Aldrich.

For $Nd_2O_3$ synthesis, neodymium nitrate solution (0.2 mol/L) and 1% (w/v) sodium alginate solution were prepared by dissolving in bidistilled water. Neodymium alginate beads of average diameter 1 mm were produced by dropwise addition of sodium alginate solution to neodymium nitrate solution, using a syringe which has a stainless-steel needle. The prepared neodymium alginate beads were separated from the solution, placed in a porcelain crucible, and heated at 500 °C for 24 h and a bluish powder was formed. The same procedure was used to synthesis $Er_2O_3$ and at the end of the synthesis a pinky powder was formed. To investigate the effect of annealing on the nanocrystals structure, the nanocrystals were annealed at 800$^{o}$C for 24 hours.

**Synthesizes of $Nd_2O_3$ and $Er_2O_3$ nanocrystals doped PMMA:** Methyl methacrylate (MMA) were used as

monomer, azobisisobutyronitrile (AIBN) were used as initiator of polymerization. MMA was passed through a commercially available (Sigma-Aldrich) inhibitor column to remove the inhibitors. AIBN were used as received without any further purification. All chemicals were obtained from Sigma-Aldrich. 1 mL of the resulting uninhibited MMA solution was poured into a glass tube, to which we added AIBN (0.001 AIBN/MMA molar ratio) as the initiator to begin the polymerization. After stirring well, rare earth oxide nanocrystals ($Nd_2O_3$ or $Er_2O_3$) were added in 1% weight ratio with respect to the monomer solution. The polymerization process was performed in an ultrasonic bath. The final solution was stirred well with ultrasonic bath at 60°C. The polymerization process begins approximately in two hours. The solution is heated for 4 hours at the same temperature and then allowed to cool overnight. The solid rare earth oxide nanocrystalline doped PMMA sample was cut and polished. In the same method, a reference sample of pure PMMA was made with AIBN as initiator and MMA as monomer for a comparison study of the absorption spectra of PMMA doped with rare earth oxide nanocrystals.

## 2.2 Structural Characterization and Spectroscopic Measurements

X-ray diffraction (XRD) patterns of $Nd_2O_3$ and $Er_2O_3$ nanocrystal powder were collected by Bruker AXS D8 diffractometer for a step size of 0.01°/2θ, between 20 and 90°; using CuKα (λ=1.54184 Å) monochromatic radiation, operating at I=10 mA, V=30 kV. The average particle sizes of the powders were estimated using the Scherrer equation [4].

$$L = \frac{K\lambda}{\beta \cos\theta} \tag{1}$$

where L is the average size of the ordered (crystalline) domains, $K$ is a dimensionless shape factor that 0.89 for spherical particles ($0.89 < K < 1$), $\lambda$ is the X-ray wavelength, $\beta$ is the width of the peak at half maximum (FWHM) intensity of specific phase in radians, and $\theta$ is the center angle of the considered Bragg reflection.

Absorption spectra were taken to identify the absorption lines of $Nd^{3+}$ and $Er^{3+}$ ions dispersed in PMMA matrix. Absorption measurements were recorded using Varian Cary 100 Bio UV-Vis spectrophotometer between 400-900 nm at room temperature.

The emission spectra of $Nd_2O_3$ doped PMMA samples collected between 850 and 1550 nm wavelength at room temperature. To collect the emission spectra a diode laser with 808 nm wavelength as excitation source from Apollo Instruments (Model no: S30-808-6), a monochromator (Princeton Instruments - model SP2500i) and Acton series (ID441-C Model) InGaAs detector were used. For $Er_2O_3$ doped PMMA samples, the emission spectra between 1000-1700 nm wavelength region were collected using an Apollo Instruments CNI Model infrared diode laser operating at 980 nm as an excitation source, and an InGaAs detector from Acton series (ID441-C Model) for the detection.

# 3 RESULTS AND DATA ANALYSIS

## 3.1 Physical Properties

The wavelength dependent refractive index of the samples were determined using Sellmeier's dispersion equation

$$n^2(\lambda) = 1 + \frac{B_n \lambda^2}{\lambda^2 - C_n} \tag{2}$$

where λ is in microns, and $B_n$, $C_n$ are Sellmeier's coefficients [5, 6]. An effective refraction index, $n_{eff}$, should be calculated using the equation given below when the nanoparticle average size is much smaller than the wavelength of light and the rare earth nanoparticles occupy only a small fraction of the total volume of polymer matrix.

$$n_{eff} = x.n_{nanoparticle} + (1-x).n_{PMMA} \tag{3}$$

where $x$, *filling factor*, represents the fraction of space is occupied by rare earth oxide nanoparticles in the PMMA matrix [7, 8]. The effective refractive indices at 632 nm of rare earth oxide doped PMMA samples are tabulated in Table 1.

| Sample | $n_{eff}$ (at 632 nm) |
|---|---|
| 1% $Nd_2O_3$ doped PMMA | 1.5384 |
| 1% $Er_2O_3$ doped PMMA | 1.5480 |

Table 1: The effective refractive indices at 632 nm of rare earth oxide doped PMMA

## 3.2 Structural Characterization

The XRD pattern of annealed and non-annealed $Nd_2O_3$ nanopowders are given in Figure 1.

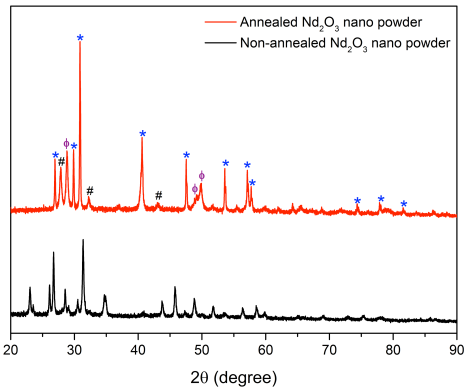


Figure 1: XRD pattern of annealed and non-annealed $Nd_2O_3$ nanocrystalline powder.

The XRD pattern of the $Nd_2O_3$ powder contains two crystalline phases that were identified to be the hexagonal phase and cubic phase. The hexagonal phase was marked with the star (*) symbol, the peak positions correspond well to the standard card with PDF#00-041-1089 according to JCPDS (Joint Committee for Powder Diffraction Data). The number sign (#) was used to label the peaks related to the cubic phase of $Nd_2O_3$ nanocystalline powder and, the peak positions correspond well to the standard card with PDF#03-065-3184.

It is known that the rare earth oxides based on the rare earth elements with an atomic number Z>62 form in a cubic crystalline phase, and those with Z<62 form in two crystalline phases which are cubic and hexagonal phases [9, 10]. The peaks observed in addition to those of hexagonal and cubic phases, demonstrated with phi ($\phi$) symbol, corresponded well to the standard card with PDF#01-083-2035 which is due to the hydration of $Nd_2O_3$. The absorption of water vapor by $Nd_2O_3$ leads to the formation of $Nd(OH)_3$ [11, 12]. The peak positions observed in the XRD pattern of non-annealed $Nd_2O_3$ powder correspond well with those of $Nd_2O_2(CO_3)$ crystalline phase (PDF#01-070-2152). It has been reported that $Nd_2O_2(CO_3)$ peaks stem from the combination of alginic acid $(C_6H_8O_6)_n$ and $Nd(NO_3)_3$. This combination leads to the formation of $Nd_2O(CO_3)_2$. As the temperature of $Nd_2O(CO_3)_2$ increases to 450-480°C since the synthesis were performed at 500°C, a transformation from $Nd_2O(CO_3)_2$ to $Nd_2O_2(CO_3)$ was observed by losing a $CO_2$ group. In addition, a second weight loss that results in losing the $CO_2$ group, was observed at 600-750°C hence, the formation of $Nd_2O_3$ above 750°C was occurred [13]. As it can be seen from the Figure 1, the XRD patterns of annealed and non-annealed $Nd_2O_3$ powders confirm the transformation of the $Nd_2O_2(CO_3)$ crystalline phase to the $Nd_2O_3$ nanocrystalline phase with heat treatment at 800°C for 24h.

The XRD pattern of annealed and non-annealed $Er_2O_3$ nanopowders are given in Figure 2.

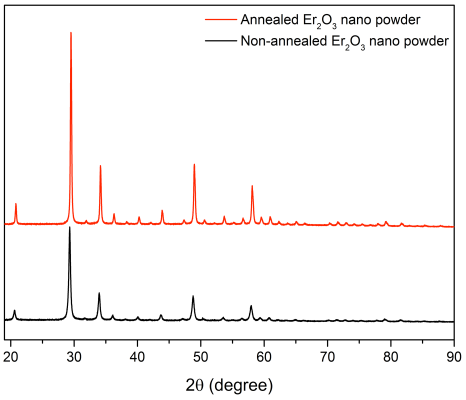


Figure 2: XRD pattern of annealed and non-annealed $Er_2O_3$ nanocrystalline powder.

The crystalline phase of $Er_2O_3$ powder is cubic. The peak positions correspond well to the standard card with PDF#01-074-1983.

The particle sizes of the powders were calculated using the Scherrer equation. The average crystalline size of annealed and non-annealed $Nd_2O_3$ powders were calculated as 46 nm and 30 nm, respectively. For $Er_2O_3$ nanopowders, the average crystalline size were calculated as 38 nm and 24 nm, respectively. It has been reported that the particle size was effectively controlled by synthesis and/or annealing temperatures and the particle size increases by increasing the synthesis and/or annealing temperatures [14].

## 3.3 Absorption Measurements

Figure 3 shows the optical absorption spectra of $Nd_2O_3$ embedded PMMA nanocomposite sample in the visible and near infrared regions at room temperature. Eleven absorption bands corresponding to the ground state absorption ($^4I_{9/2}$), of $^2P_{1/2}$, $^4G_{11/2}$ + $^2D_{3/2}$, $^2G_{9/2}$ + $^2K_{15/2}$, $^4G_{9/2}$, $^4G_{7/2}$ + $^2K_{13/2}$, $^4G_{5/2}$ + $^2G_{7/2}$, $^2H_{11/2}$, $^4F_{9/2}$, $^4S_{3/2}$ + $^4F_{7/2}$, $^4F_{5/2}$ + $^2H_{9/2}$ and $^4F_{3/2}$ levels centered at about 434, 463, 477, 515, 533, 594, 630, 687, 752, 809, and 884 nm were identified, respectively. It can be seen from the figure that some of the absorption bands of the adjacent energy levels such as the $^4G_{5/2}$ + $^2G_{7/2}$, $^4S_{3/2}$ + $^4F_{7/2}$, $^4F_{5/2}$ + $^2H_{9/2}$ levels overlap due to the crystalline field effect.

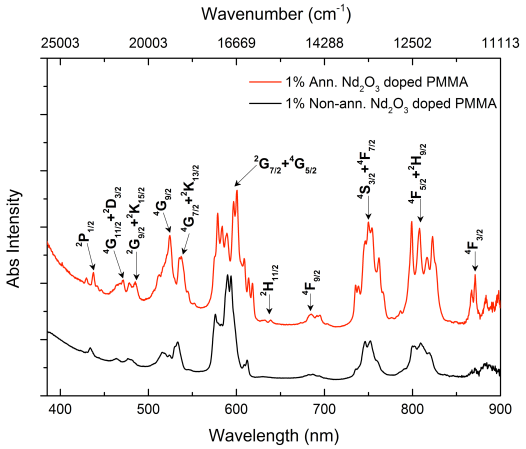


Figure 3: Absorption spectra of 1% (wt) annealed and non-annealed $Nd_2O_3$ doped PMMA sample.

Figure 4 shows the optical absorption spectra of $Er_2O_3$ embedded PMMA nanocomposite sample in the visible and near infrared regions at room temperature. Eight absorption bands corresponding to the ground state absorption ($^4I_{15/2}$), of ($^2G$, $^4F$, $^2H$)$_{9/2}$, $^4F_{3/2}$, $^4F_{5/2}$, $^4F_{7/2}$, $^2H_{11/2}$, $^4S_{3/2}$, $^4F_{9/2}$, and $^4I_{9/2}$ levels centered at about 408, 444, 454, 489, 522, 539, 654, and 800 nm were identified, respectively.

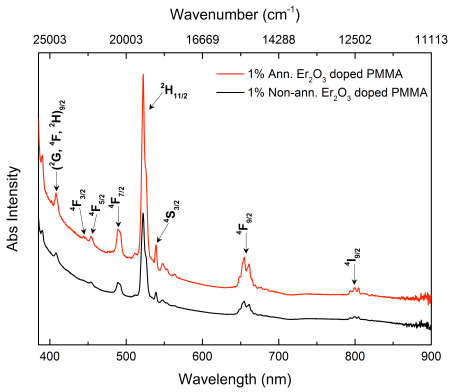


Figure 4: Absorption spectra of 1% (wt) annealed and non-annealed $Er_2O_3$ doped PMMA sample.

## 3.4 Emission Measurements

The emission spectra of 1% $Nd_2O_3$ doped PMMA samples were collected between 850 and 1550 nm wavelength at room temperature by using diode laser with 808 nm wavelength as an excitation source are given in Figure 5.

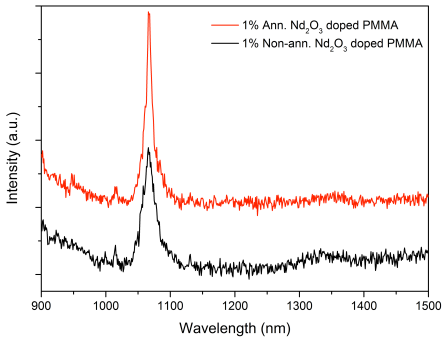


Figure 5: Near infrared emission spectra of 1% annealed and non-annealed $Nd_2O_3$ doped PMMA samples at room temperature.

The emission spectra of 1% $Er_2O_3$ doped PMMA samples were collected between 1000 and 1700 nm wavelength at room temperature by using diode laser with 980 nm wavelength as an excitation source are given in Figure 6.

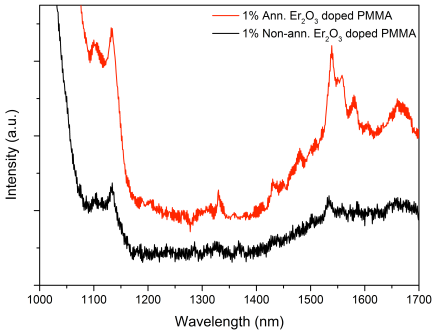


Figure 6: Near infrared emission spectra of 1% annealed and non-annealed $Er_2O_3$ doped PMMA samples at room temperature.

# 4 CONCLUSION

$Nd_2O_3$ and $Er_2O_3$ powders in the form of nanocrystals were synthesized by thermal decomposition process and were then embedded in PMMA host matrix. XRD measurements of the $Nd_2O_3$ nano-powders show that the crystalline phase is transformed from pure hexagonal $Nd_2O_2(CO_3)$ to cubic and hexagonal $Nd_2O_3$ under the heat treatment at 800°C for 24 hours. For $Er_2O_3$ nano-powders only one phase, cubic phase, was observed.

According to the absorption spectra of $Nd_2O_3$ doped PMMA eleven absorption bands obtained. For $Er_2O_3$ doped PMMA sample, eight absorption bands obtained. According to emission spectra of both $Nd_2O_3$ and $Er_2O_3$ doped PMMA sample, the heat treatment causes a sharper emissions.

# REFERENCES


[1] W. Luo, J. Liao, R. Li, and X. Chen, Phys. Chem. Chem. Phys., vol. 12, pp. 3276–3282, 2010.

[2] W. H. Wong, K. K. Liu, K. S. Chan, and E. Y. B. Pun, J. Cryst. Growth, vol. 288, no. 1, pp. 100–104, 2006.

[3] L. H. Slooff, A. Polman, S. I. Klink, G. A. Hebbink, L. Grave, F. C. J. M. Van Veggel, D. N. Reinhoudt, and J. W. Hofstraat, Opt. Mater. (Amst)., vol. 14, no. 2, pp. 101–107, 2000.

[4] P. Scherrer, Nachrichten von der Gesellschaft der Wissenschaften zu Göttingen, Math. Klasse, vol. 1918, no. 1916, pp. 98–100, 1918.

[5] Mohammed, A.E.N.A., A.E.F.A. Saad, and A.N.Z. Rashed, International Journal of Physical Sciences, 2009. 4(4): p. 205-211.

[6] R.D. Shannon, et al., Journal of physical and chemical reference data, 2002. 31(4): p. 931-970.

[7] R. Meltzer, et al., Physical Review B, 1999. 60(20): p. R14012.

[8] R. Meltzer, et al., Journal of Luminescence, 2001. 94: p. 217-220.

[9] T. Busani, et al., ECS Transactions, 2006. 1(5): p. 331-340.

[10] M. da Silva, et al., Journal of thermal analysis and calorimetry, 2009. 99(2): p. 385-390.

[11] M. Nagao, et al., Langmuir, 2003. 19(22): p. 9201-9209.

[12] H. Hamano, et al., Langmuir, 2000. 16(17): p. 6961-6967.

[13] Y. Zhang, et al., Green Chemistry, 2015. 17(6): p. 3600-3608.

[14] G. Bilir, et al., Applied Physics A, 2014. 115(1): p. 263-273.